Flexural capacity of reinforced concrete slabs retrofitted with ultra-high-performance concrete and fiber-reinforced polymer

Viet Hai Hoang[1] · Tu Anh Do[1] · Anh Tuan Tran[1] · Xuan Huy Nguyen[2]

Abstract

In this study, a new method for strengthening and retrofitting the flexural capacity of reinforced concrete (RC) slabs using ultra-high-performance concrete (UHPC) and fiber-reinforced polymer (FRP) is proposed. The effectiveness of the strengthening method was investigated through experimental studies. Eight RC slabs were tested consisting of the control slab (without strengthening), a slab strengthened with FRP at the bottom, and six slabs retrofitted with 30-mm-, 40-mm-, and 50-mm-thick UHPC layers on the top and also strengthened with FRP at the bottom. The flexural capacities of the slabs were determined using four-point bending tests. Detailed flexural behaviors including cracking patterns, strain distribution, and ductility of the test slabs were examined and compared. The findings demonstrated that the incorporation of UHPC layers in the compressive zone of the RC slabs played a crucial role in substantially increasing their strengths (from 31.48 to 64.09%) and changing the modes of failure and cracking patterns within the composite slabs. Moreover, the combined use of UHPC in the compressive zone and FRP in the tension zone resulted in a remarkable increase (from 10.35 to 40.08%) in the flexural capacity, and about 1.9–2.3 times reduction in the maximum deflection compared to slabs using only UHPC in the compressive zone.

Keywords Ultra-high-performance concrete · Fiber-reinforced polymer · Flexural capacity · Reinforced concrete slabs

Introduction

Concrete structures such as in bridges undergo degradation over time due to various factors including aging, exposure to harsh environmental conditions, and extreme events such as earthquakes and vehicular impacts. Rehabilitating deteriorated concrete structures to restore their original design capacities is often considered to be a more practical and cost-effective approach compared to demolition and reconstruction. Illustrations of the degradation of reinforced concrete (RC) slabs in truss bridges leading to damage of the asphalt concrete [1] in the bridge deck are shown in Figs. 1 and 2. Recently, a series of new reinforcing materials, such

as ultra-high-performance concrete (UHPC) [2–6], textile-reinforced concrete (TRC) [7], steel plates [8], and FRP [9], have emerged and been used in the rehabilitation and reinforcement of civil engineering structures.

UHPC possesses superior mechanical properties when compared to conventional concrete. It exhibits remarkable characteristics such as an exceptionally high compressive strength (ranging from 120 to 200 MPa), excellent tensile strength, high crack resistance (7–15 MPa), and excellent resistance to corrosion due to its low water permeability and low chloride penetration [10, 11]. The presence of steel fibers in the concrete mixture improves its ductility, enhances its flexibility and bond strength between the concrete and steel reinforcement, and reduces crack widths. With such exceptional properties, UHPC is considered as one of the valuable solutions for repairing and constructing various transportation infrastructures.

UHPC has recently gained prominence as a promising option for retrofitting and repairing existing RC elements. Brühwiler Eugen [12] has introduced innovative concepts for leveraging the extraordinary properties of UHPC to enhance specific structural components. The application of UHPC

✉ Viet Hai Hoang
hoangviethai@utc.edu.vn

1 Faculty of Civil Engineering, University of Transport and Communications, 3 Cau Giay, Lang Thuong, Dong Da, Hanoi, Vietnam

2 Faculty of Construction Engineering, University of Transport and Communications, 3 Cau Giay, Lang Thuong, Dong Da, Hanoi, Vietnam

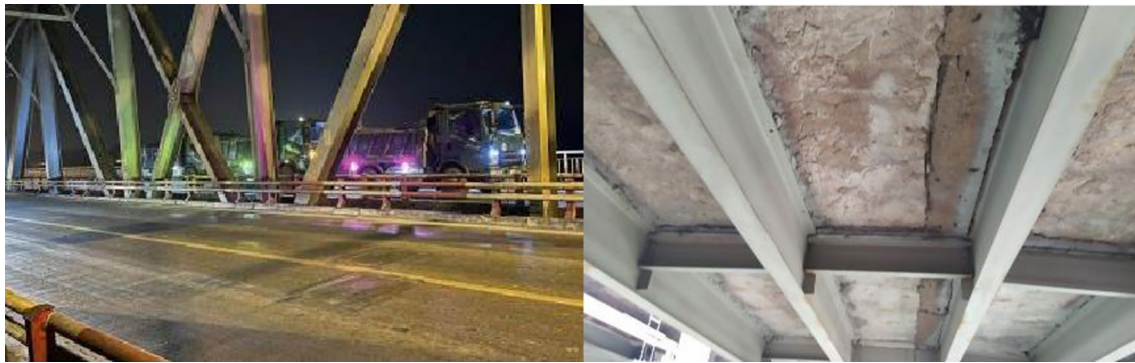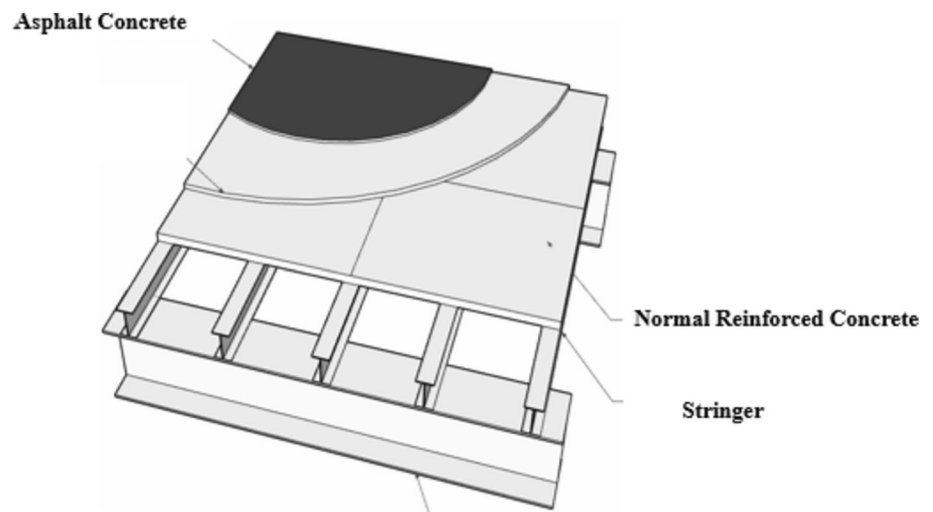**Fig. 1** Example of concrete bridge deck in truss bridge

Fig. 2 The structure of Chương Dương Bridge (in Hanoi, Vietnam) and some defaults

has shown substantial promise, with the technology now being well-established for use in cast in situ and in precast structures.

To assess the effectiveness of UHPC in strengthening RC structures, several experimental studies using UHPC to reinforce RC structures have been conducted, for example, in Refs. [13–16]. For instance, Noshiravani and Brühwiler [17] analyzed the flexural behavior of RC specimens strengthened with UHPC overlays. The results indicated that the UHPC overlays enhance ultimate loads, stiffness, and reduce cracking behavior of the tested specimens. Another investigation was carried out by Yin Hor et al. [18] and Al-Osta et al. [19] using UHPC to rehabilitate and strengthen RC beams in tension zone. The results showed that the application of UHPC reduced diagonal cracks and led to the development of more verticals cracks in comparison with control RC slabs. Nevertheless, limited attention has been given to assessing the impact of UHPC in the compression zone.

FRP has gained increasing popularity in the retrofitting of reinforced concrete (RC) bridges, serving as a replacement for steel in the tension zone through near-surface mounting (NSM) or external bonding (EB) reinforcement techniques [20–22]. In this method, FRP sheets or plates are typically affixed to the tension surface of beams or slabs to enhance bending strength. Alternatively, they can be applied to the sides of slabs to improve shear strength, following the preparation of the concrete surface through grinding and cleaning. The application process involves the use of epoxy resin material. Ensuring a secure bond between the FRP and the RC structure. The primary advantage of this technique lies in its rapid and straightforward installation, while a notable drawback emerges when a substantial amount of FRP is required. This can lead to an increased external reinforcement thickness, thereby elevating the risk of nonconventional debonding failure [23].

To effectively enhance the capacity of RC structures, it is imperative to use a material that offers the higher ductility while maintaining substantial strength. UHPC emerges as a promising solution owing to its remarkable ductility when applying in compression and tension zones. However, the behavior of the composite structures affected

by the addition of a UHPC layer in the compression zone remains inadequately elucidated. Notably, there is a dearth of studies concerning composite members that incorporate an additional UHPC overlay and an FRP layer in the tension zone applied to existing RC members. Recently, Long Liu et al. [24] have employed a novel composite reinforcement technique, which involves the incorporation of a UHPC layer in the compression zone, while using CFRP strips or CFRP bars in the tension zone of RC beams. Their research demonstrates that their method significantly enhances the flexural capacity of RC beams, surpassing that of the control beam by 132.3% and outperforming those of the RC beams reinforced solely with CFRP strips/CFRP bars by 7.8%. Nevertheless, it is important to note that the influence of the thickness of the UHPC layer on the bending behavior of the RC beams has yet to be fully elucidated in this experimental study. Additionally, the installation of CFRP bars using the NSM technology is very difficult and not suitable for concrete bridge decks. For this type of structures, employing the EB method is more appropriate. Actually, the behavior of concrete slab structures differs from that of concrete beams due to differences in thickness and typical reinforcement arrangements [25]. Therefore, there is a need to study the mechanical behavior of the bridge deck structures when supplementing a UHPC layer in the compression zone or/ and combining with FRP using the EB technology.

This research aims to determine the flexural capacity of composite UHPC-RC slabs-FRP. To achieve this goal, experimental studies were conducted on various configurations of the retrofitting UHPC layer in the compression zone and the strengthening FRP in the tension zone of the tested RC slabs. The new method for strengthening and retrofitting the flexural capacity of RC slabs is described. Sections "Materials and test specimens" and "Four point bending test" present details of the equipment and test setup. The test results, which focus on the mechanical behavior of slabs under loading, distribution of strain at mid-span, and failure modes of slabs, are discussed in Section "Results and discussion." Section "Conclusions" summarizes the research findings and offers recommendations for future studies in this field.

Materials and test specimens

Test specimens

This experimental investigation was conducted on eight slabs with different composite UHPC-RC slabs-FRP configurations. To evaluate the separate or simultaneous effects of UHPC and FRP on the structural behavior, two series of mechanical testing were carried out. The first series used UHPC as a rehabilitative and retrofitting material for the overlay of concrete slabs, labeled as UE. The second series, where UHPC was used for the rehabilitation and retrofitting of the overlay, and FRP was applied as the external bond in the tension zone of the slabs, was labeled as UE-F. The UE series consisted of four slabs, while the UE-F series also comprised four slabs. All slabs measured 1800 mm in length and 360 mm in width. There were three RC slabs strengthened with different thicknesses of 30 mm, 40 mm, and 50 mm of UHPC layer(s) (Fig. 3). Full dimensions of the different composite UHPC-RC slabs-FRP configurations are illustrated in Fig. 3.

The use of UHPC in the compression zone of RC slabs as a new material for the repair, rehabilitation, and retrofitting of this structure was investigated in the UE series. Normally, deteriorated concrete in the protective concrete cover of RC slabs will be removed, and a new material will be applied for restoring this concrete cover. In this series, three different thicknesses of UHPC layers were examined to reflect various repair, retrofitting cases. All strengthened slab specimens were produced by remaining 110 mm in height with normal concrete (NC) and using the different UHPC layers from 30 to 50 mm in thickness poured into the surface of NC. For example, the specimen "UE-30" described a RC slab with deteriorated concrete in the protective concrete cover removed and replaced by a UHPC layer with the thickness of 30 mm. To prevent any slippage at the interface of the RC slab surface and the UHPC layer, a series of steel bars with a 10-mm diameter were positioned prior to pouring of the normal concrete. Refer to Figs. 3 and 7a for details regarding their placement and dimensions. All the slabs in the two series had six longitudinal reinforcements with a 12-mm diameter (6D12) arranged at the top and bottom in their cross-sections. Slab UE-50 consisted of 50-mm-thick UHPC layer, and this layer was strengthened with 6D10 longitudinal reinforcement. The previous studies have demonstrated the necessity of employing a reinforced to enhance the capacity of the 50-mm-thick UHPC layer [12]. To simulate the structural slabs, no transverse reinforcement was designed, but to prevent the concrete failure at the supports position under loading, four transverse rebars with a diameter of R6 mm were reinforced at the support positions. The position of reinforcement of all slabs is detailed in Fig. 3.

The UE-F series comprised four slabs, similar to the UE series, but with the addition of FRP in the tension zone. The detailed dimensions and reinforcement of slab specimens are summarized in Table 3.

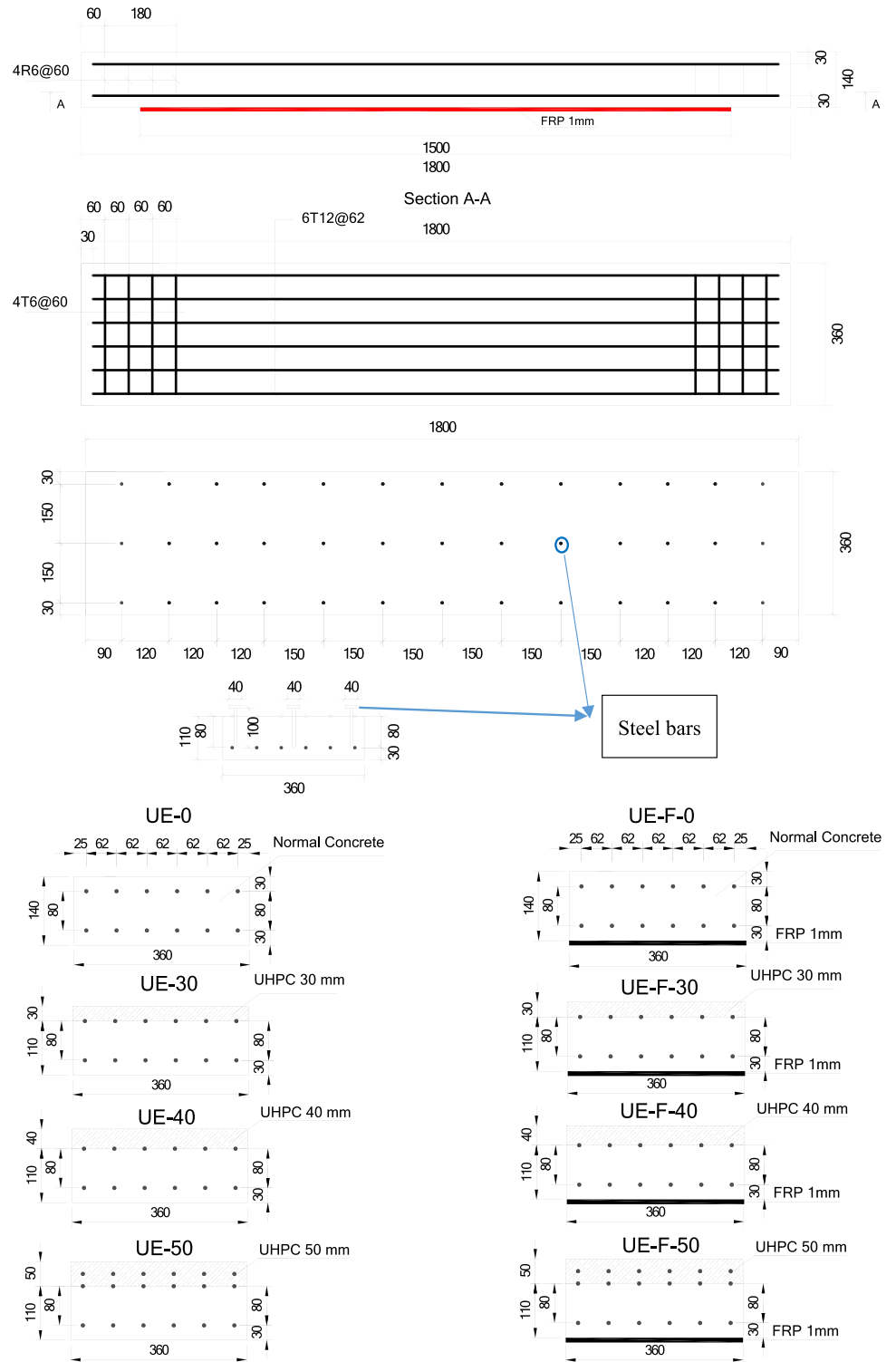**Fig. 3** Details of UE and UE-F series composite UHPC-concrete-FRP configurations

Table 1 Mix proportion of the UHPC

Cement (kg/m^3)	Quartz sand (kg/m^3)	Silica fume (kg/m^3)	Superplasticizers (liter/m^3)	Water (kg/m^3)	Steel fibers (kg/m^3)
788	1095	252	23.6	176.8	156

The retrofitted specimens for both series underwent a two-step pouring process. Initially, the NC was poured, followed by the application of a UHPC mixture on the top surface of the NC. To determine the compressive strength of the NC, three standard cylinders, each with a height of 300 mm and a diameter of 150 mm, were utilized. All slab specimens and cylinders were kept in a controlled room environment, covered with film for 7 days to maintain constant moisture. The average compressive strength of the NC at 28 days was measured at 37.6 MPa.

After 3 days, the NC had hardened. Consequently, its top surface was intentionally roughened to create an optimal bonding surface with the subsequent layer (refer to Fig. 7a). The mix proportions of UHPC are detailed in Table 1. Figure 7 displays the test specimens before and after the pouring of the UHPC paste. In Fig. 7c, the bonding of the FRP sheet to the bottom of the slabs in the UE-F series is illustrated.

Ultra-high-performance concrete (UHPC)

De Larrard [26] proposed the compressible packing model (CPM) to design the mixing of cement-based materials [27–29]. The method and mix design of UHPC in this study used the modified Anderson and Andresen model to optimize a densely packed particle skeleton of UHPC [30, 31]. The UHPC was composed of main constituent materials, and the mix proportions used to produce UHPC are detailed in Table 1. The steel fibers used had a tensile strength greater than 2000 MPa, a diameter of 0.2 mm, and a length of 12 mm. The mass of steel fibers added was calculated to ensure a content of 2% (by volume of concrete), as proposed by several studies worldwide [10], to achieve a tensile strength of the material greater than 8 MPa. The average compressive strength of the tested UHPC cylinders at 28 days was 127.6 MPa, with a tensile strength of 12.1 MPa [32].

FRP

The test slabs underwent strengthening with CFRP produced by Tyfo SCH-41. The CFRP sheets had a thickness of 1 mm and a width of 360 mm, exhibiting an ultimate tensile strength (f_u) of 986 MPa, a tensile modulus of elasticity of 95.8 GPa, and an elongation of 1.01%. The adhesive used for bonding the CFRP was Tyfo S, specifically designed for this purpose. Key properties of the FRP are outlined in Table 2.

The carbon laminate had a thickness of 1.00 mm, as indicated in Fig. 7c, with a length of 1500 mm and a width of 360 mm.

Four-point bending test

A four-point bending test was employed to assess the mechanical behavior of the RC slabs strengthened with UHPC and FRP under various loads [35]. This allowed for the determination of the stress and strain evolution of this hybrid structure during loading. The slabs were positioned on two supports, as shown in Fig. 4. The distance between the two adjacent supports was 1530 mm, which corresponds to the actual longitudinal slabs spacing in the deck slabs of Chuong Duong Bridge (Fig. 2). A 3000-kN hydraulic jack, operating at a loading rate of 0.1 kN/s, was employed to apply the load. Additionally, a load cell with a capacity of 500 kN was employed to measure the applied load. Two concentrated loads with a distance of 510 mm

Table 2 Properties of composite sheet laminate

Item	Test value	Design value	Test method
Ultimate tensile Strength in primary fiber direction (MPa)	986	834	D3039 [33]
elongation at break (%)	1.01	0.85	D3039 [33]
Tensile modulus (GPa)	95.8 GPa	82	D3039 [33]
Flexural strength (MPa)	123.4	104.8	D790 [34]
Flexural modulus (GPa)	3.12	2.65	D790 [34]
Nominal laminate thickness	1.0 mm	1.0 mm	

Fig. 4 Point of view of four-point bending test
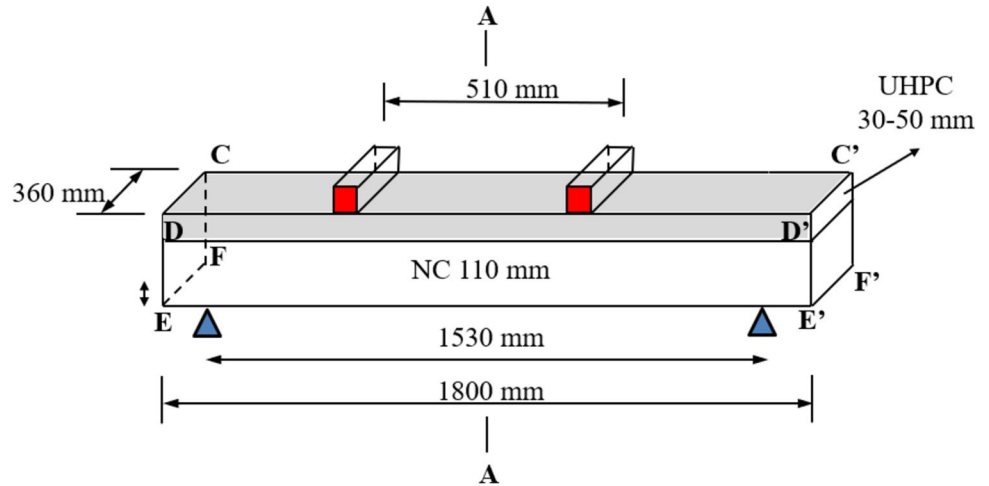
Fig. 5 Test specimen geometry

Specimen label	b (mm)	h (mm)	UHPC thickness, h_U (mm)	FRP thickness, h_{FRP} (mm)	Longitudinal reinforcement		
					Top slabs		Bottom slabs
					A'_{sU}	A'_s	A_s
UE-0	360	140	–	–	–	6T12	6T12
UE-30	360	140	30	–	–	6T12	6T12
UE-40	360	150	40	–	–	6T12	6T12
UE-50	360	160	50	–	6T10	6T12	6T12
UE-F-0	360	140	–	1		6T12	6T12
UE-F-30	360	140	30	1		6T12	6T12
UE-F-40	360	150	40	1		6T12	6T12
UE-F-50	360	160	50	1	6T10	6T12	6T12

Table 3 Geometry and reinforcement of test specimens

Fig. 6 Positions of strain gauges: **a** Section CC'F'F and **b** Section CC'D'D
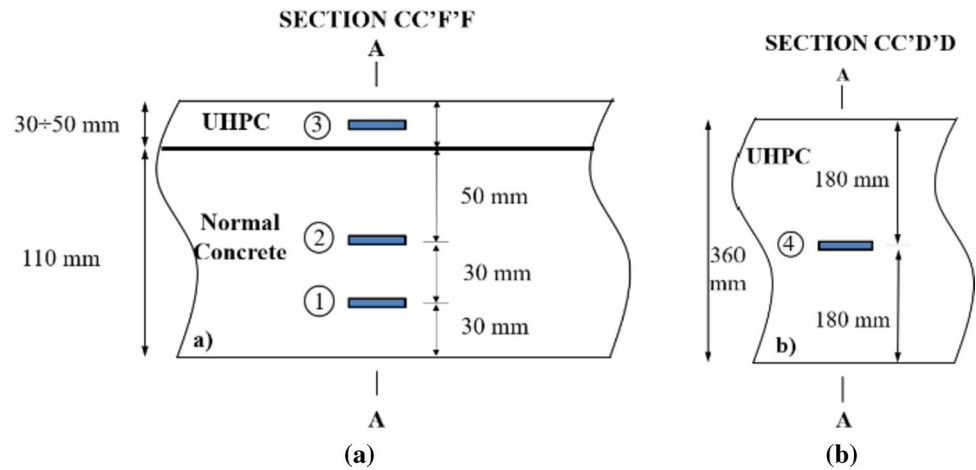
were applied to the slabs via a metallic plate until they failed, as depicted in Fig. 5.

An LVDT was used to measure the vertical deflection at mid-span. Meanwhile, strain gauges were utilized to measure the external longitudinal strains of both concrete and UHPC. Figure 4 displays a specimen with instrumentation setup for testing. The tests were conducted at a loading rate of 0.1 kN/s (Table 3).

Table 4 Summary of test results

Specimen label	Ultimate		Yield		Ductility index μ (μ$_e$)	Mode of failure
	L$_u$ (kN)	δ$_u$ (mm)	L$_y$ (kN)	δ$_y$ (mm)		
UE-0	148.35	15.65	111.26	9.8	1.59	Shear
UE-30	195.06	36.47	146.29	11.16	3.26	Flexure
UE-40	230.05	35.18	172.53	11.66	3.01	Flexure
UE-50	243.43	33.98	182.57	10.85	3.13	Flexure
UE-F-0	201.96	13.48	151.47	9.56	1.41	Debonding- shear
UE-F-30	272	17.56	204	11.51	1.52	Debonding- shear
UE-F-40	253.88	13.98	190.41	9.83	1.41	Debonding- shear
UE-F-50	341	17.84	255.75	11.02	1.61	Debonding- shear

where L$_u$: ultimate load, L$_y$: load at yielding, δ$_y$: mid-span deflection at yielding determined from load versus mid-span displacement curve, δ$_u$: mid-span deflection at ultimate load determined from load versus mid-span displacement curve, and μ$_d$: displacement ductility index
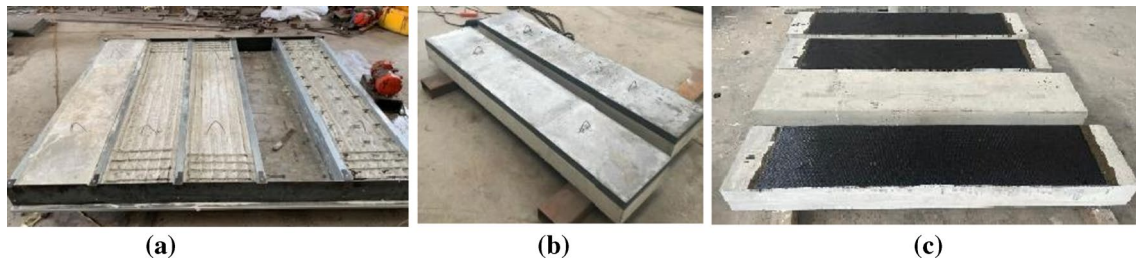

(a)   (b)   (c)

Fig. 7 **a** Control slabs and RC slabs before UHPC layer pouring, **b** UHPC-RC specimens, and **c** UHPC-RC-FRP specimens

Fig. 8 Modes of failure and development of crack observed in the UE series

Figure 6 depicts the locations of the strain gauges (sensors) installed on the front faces of the specimen (DD'EE' and CC'FF'). KYOWA strain gauges with a 60-mm gauge length are used. Before attaching the gauges using adhesive, the concrete surface underwent polishing with sandpaper and cleaning. Four strain gauges, labeled with numbers from 1 to 4, were then affixed to the concrete surface at Sections A-A, as demonstrated in Fig. 6.

Results and discussion

UE Series

Modes of failure

The ultimate load in the UE series and their modes of failure are summarized in Table 4 (Fig. 7). In addition, to investigate clearly the failure behavior, the development of cracks during loading in each slab was noted, as shown in Fig. 8. Slab UE-0 was a control slab made of NC. It failed in shear, and an ultimate load of 148.35 kN was recorded. The mode of failure was sudden and brittle with main diagonal cracks.

All slabs strengthened with UHPC showed no debonding at the interface between the UHPC layer and NC. Slab UE-30 was retrofitted with a 30-mm-thick layer of UHPC to simulate the replacement of the concrete cover of the slab with UHPC. It failed in flexure with longitudinal reinforcement deformed beyond the allowable limit at the tension zone, as shown in Fig. 8. This slab exhibited higher ductility than slab UE-0. Some oblique cracks appeared in the shear zone, but no shear failure occurred. Compared to

the reference slab UE-0, slab UE-30 failed at a higher load with an ultimate load of 195.06 kN.

Slab UE-40 was retrofitted with a UHPC layer of 40 mm. This slab failed in bending, and an ultimate load of 230.05 kN was determined from the test. Slab UE-50 was strengthened with a UHPC layer of 50 mm. The failure mode was a ductile flexural failure followed by a main crack in bending at the bottom of the RC slab, going up to the UHPC layer. Based on the results from slabs UE-30, UE-40, and UE-50, it is evident that the ultimate load increased with increasing thickness of UHPC in the compression zone. An ultimate load of 243.43 kN was recorded with slab UE-50.

Logically, the ultimate load of specimens increased with an increase in the thickness of UHPC. Strengthening with a 30-mm, 40-mm, and a 50-mm UHPC overlays induced an increase in the ultimate load capacity by 31.48%, 55.07%, and 64.09%, respectively.

Load vs mid-span displacement curves

The evolution of mid-span deflection under loading for the UE series of specimens is plotted in Fig. 9. The curves were obtained from the LVDTs installed at mid-span of slabs, as described in Section "Four point bending test."

As shown in Fig. 9, as the load increases, the deflection at the mid-span slab also increases. When the load reaches from 35 to 50 kN, cracks due to bending moment appear in the mid-span area, reducing the stiffness of the main slab. Subsequently, in the next phase as the load continues to increase, the relationship between force and deflection becomes mostly linear; however, the slope of the curve decreases. The steel reinforcement reaches the yield limit. Beyond this stage, the slab UE-0 suddenly fails due to

Fig. 9 Evolution of mid-span deflection under loading of UE series
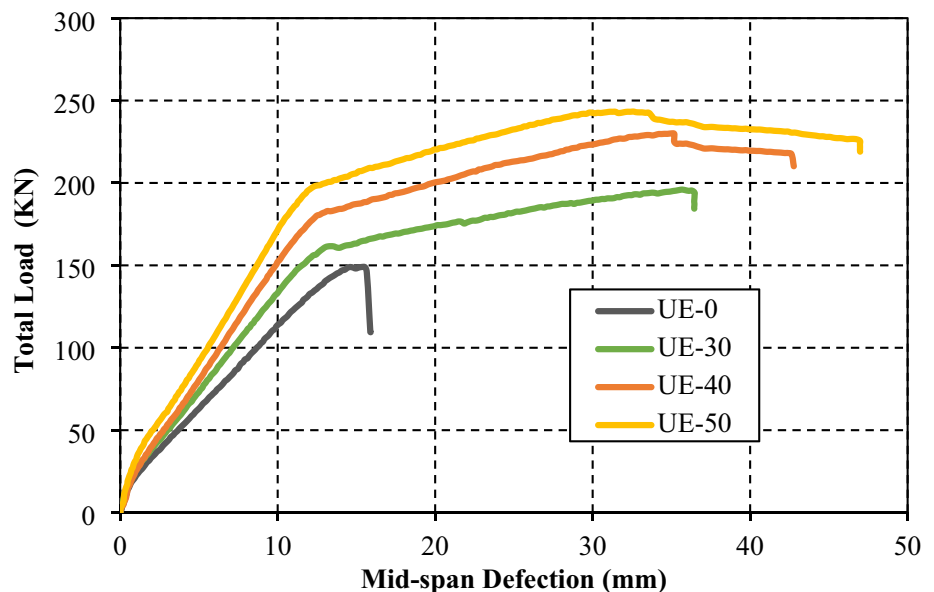
shearing. The UHPC-reinforced slabs continue to deflect under the influence of the load, but the slope of the curve decreases before failure occurs (Fig. 9).

The load–deflection curve of slab UE-0 is quasi-linear. This slab failed in brittle shear. When the compression zone was retrofitted by changing the concrete cover layer to a UHPC layer, the behavior of the slab enhanced. As shown in Fig. 9, all the hybrid UHPC-RC slabs achieved very high deflections before failure. At the ultimate load, the deflection of slab UE-30, which has the same height as slab UE-0, is 36.47 mm, which is 2.1 times larger than that of the control slab. Logically, when the height of slab UE-40 and slab UE-50 increases, their deflection at failure becomes 2.68 times and 3.12 times that of slab UE-0, respectively. This result is also consistent with the previous studies by Long Liu et al. [24] and Brühwile [12].

In the next section, the focus of structural strengthening is on the use of FRP to increase the reinforcement in the tension zone.

UE-F series

Modes of failure

As presented earlier, the UE-F series was composed of four slabs similar to the UE series. The only difference in this series was the bonded FRP at the bottom of the slabs (see Fig. 3). The modes of failure for each slab are shown in Fig. 10, and their ultimate loads and mid-span deflections at the ultimate load are summarized in Table 4.

Regardless of the introduction of FRP strengthening, all the failed slabs exhibited shear failure in the NC after the

debonding of FRP (Fig. 10). Firstly, the phenomenon of debonding of the FRP layer occurred at the support, inducing brittle slab failure. The FRP sheet actually affected the lower appearance of diagonal shear cracks and vertical bending cracks that extended up to the UHPC overlay. Typically, when debonding of the FRP sheet occurred, ultimate failure ensued suddenly. In all cases, there was no debonding failure observed between UHPC and RC at the contact interface, as depicted in Fig. 10.

Comparing Figs. 10 and 8 reveals a significant influence of the FRP layers on the ultimate strength, mid-span deflection at the ultimate load, and failure modes of the tested slabs. The FRP layers helped all slabs retrofitted with FRP increase the ultimate load while reducing the maximum deflection at ultimate flexure. For example, slabs UE-30 and UE-30-F failed at ultimate loads of 195.06 kN and 272 kN, with ultimate deflections of 36.47 mm and 17.56 mm, respectively. This can be explained by the fact that the failure in this series of slabs was controlled by the debonding of the FRP layers. The ultimate loads of slabs UE-30 and UE-30-F were about 31% and 42% higher than those of UE-0 and UE-0-FRP, respectively.

The ultimate strengths of slabs UE-F-40 and UE-F-50 were about 10.3% and 40.3% higher than that of UE-40 and UE-50, respectively. Specifically, the maximum deflection at ultimate flexure of UE-F-50 was only 17.84 mm, which is 2.63 times smaller than that of UE-50.

Load vs mid-span displacement curves

The evolution of mid-span deflection under loading in the UE-F series is illustrated in Fig. 11. These deflection curves

Fig. 10 Modes of failure and crack patterns of UE-F series

Fig. 11 Evolution of mid-span deflection under loading of UE-F series
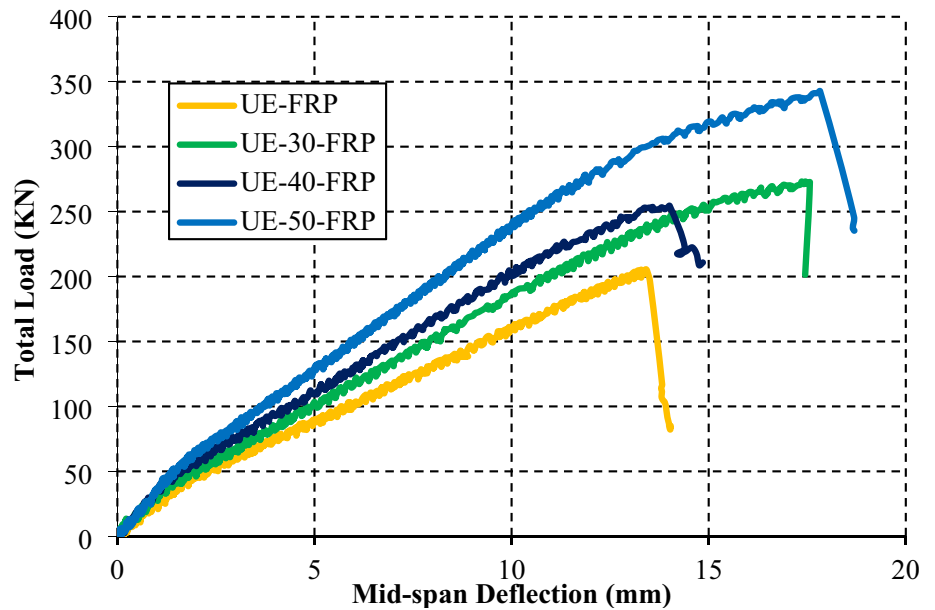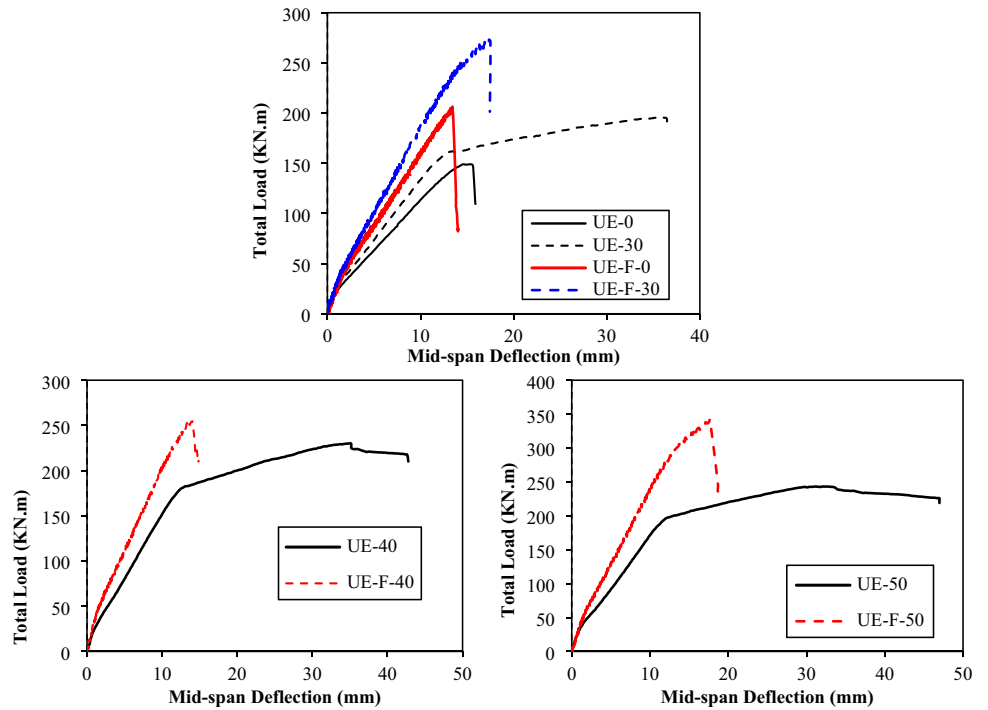

Fig. 12 Evolution of mid-span deflection under loading comparisons between UE series and UE-F series at the same height of specimen

were obtained from the LVDTs installed at the mid-span of the slabs.

Obviously, with the presence of FRP in the tension zone, the overall stiffness of the retrofitted slabs improved significantly compared with the reference slab UE-F-0. All the slabs failed in shear with diagonal shear in the NC after debonding FRP (Fig. 10).

The load–deflection curve of slab UE-F-0 is quasi-linear. The thickness of the UHPC overlay affected the stiffness of the retrofitted slabs. Increasing the thickness of UHPC layers

increases stiffness, as shown in slabs UE-F-30, UE-F-40, and UE-F-50. For example, the total loads applied to slabs UE-F-0, UE-F-30, UE-F-40, and UE-F-50 were 157 kN, 195.85 kN, 203.57 kN, and 237.68 kN, respectively, to reach a 10-mm mid-span deflection (Fig. 12). Slab UE-F-50 failed at the highest load, with an ultimate P_u of 341 kN at a maximum deflection of only 17.84 mm (Fig. 12.c). This deflection is slightly higher than the deflection of the control slab UE-0, which was 15.65 mm. However, the ultimate force of the control slab is the lowest at 148.35 kN (Table 4).
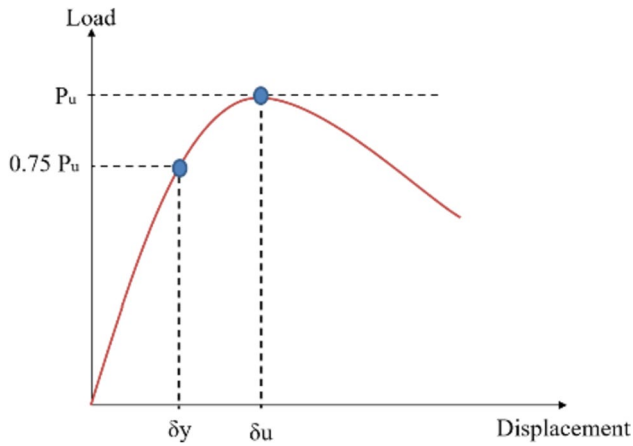
Fig. 13 Ductility calculation of specimens [36]

Figure 12.a shows the influence of FRP in the tension zone, where the ultimate loads applied on slabs UE-FRP were greater than that of UE-30, which uses only UHPC-concrete in the compression zone. The ultimate loads of both of these specimens were higher than that of the control specimen. The combination of UHPC and FRP materials significantly enhances their effectiveness in ultimate force, exhibiting respective increases of 1.83, 1.39, and 1.35 compared to slabs UE-0, UE-30, and UE-FRP (Fig. 12.a). The presence of FRP plays a crucial role in minimizing deflection corresponding to the ultimate load compared to specimens strengthened solely by the UHPC layer in the compression zone (Fig. 12.b and c). Slabs UE-F-30, UE-F-40, and UE-F-50 failed with ultimate loads 39.44%, 10.35%, and 40.08% higher than those of UE-30, UE-40, and UE-50, respectively. However, the maximum deflection at the ultimate flexure of UE-F-30, UE-F-40, and UE-F-50 is 2.07, 2.5, and 1.9 times lower compared to that of UE-30, UE-40, and UE-50.

Ductility

Ductility in a structure refers to its capacity to withstand applied loads without collapsing over a specified amount of deformation. Various models exist for characterizing the ductility of RC structures, with the most widely used model relying on deformation and expressed in terms of displacement (Eq. 1).

$$\mu_{\mathrm{d}} = \frac{\delta_{\mathrm{u}}}{\delta_{\mathrm{y}}} \tag{1}$$

where μ_{d} is the displacement ductility index, δ_{u} and δ_{y} are the displacements at the ultimate and yielding loads or moments, respectively.

In this study, the ductility indexes of the tested slabs were assessed using the load–deflection curves (Eq. 1). The ultimate displacement (δ_{u}) corresponded to the ultimate load while the yielding displacement δ_{y} was calculated based on Ref. [36], as shown in Fig. 13. Table 4 presents the mid-span deflection at yielding and ultimate loads, along with the ductility indexes for all the slabs tested.

In the UE series, the ductility indexes of the retrofitted slabs increased approximately 2 times with the presence of the UHPC overlay in the compression zone compared to the control slab. The greatest ductility index was found in slab UE-30 measuring at 3.26 (Table 4), while those of slabs UE-40 and UE-50 were 3.01 and 3.13, respectively. The flexural capacities of the slabs were limited by the tensile capacity of the longitudinal reinforcement in the bottom of the slabs. As demonstrated in the tested specimens, slabs UE-30, UE-40, and UE-50 failed in ductile flexure, with the longitudinal reinforcement deforming beyond the allowable limit in the tension zone (Fig. 8).

In terms of the strengthening type, the UE-F series exhibited lower ductility compared to the UE series. Among the UE slabs, the highest ductility was observed in slab UE-30 utilizing a 30-mm UHPC overlay. In contrast, within the UE-F slabs, the greatest ductility was found in slab UE-F-50, featuring carbon sheets bonded to slab UE-50. There were no significant variations in ductility when comparing each slab within this series. All slabs in the UE-F series demonstrated ductility exceeding 1.0.

Cross-sectional strain distribution

Figure 14 shows the strains of the composite UHPC-RC across the height at mid-span. It can be observed that all slabs conform to the plane-section assumption. The height of the compression zone decreases with the increase in loading.

For the UE series, the applied UHPC to the concrete cover resulted in a significantly enhanced strain distribution. Under the same load level, the height of the compression zone with the UHPC layer in the top slab is higher than that of the control slab. In addition, it can be observed that the height of the compression zone of slab UE-50 is larger than that of slab UE-40.

In the UE-F series, the application of FRP strengthens the slab structures by increasing the content of tensile reinforcement. This augmentation induced an increase in the neutral axis position of the section when subjected to the same load, compared to a similar slab.
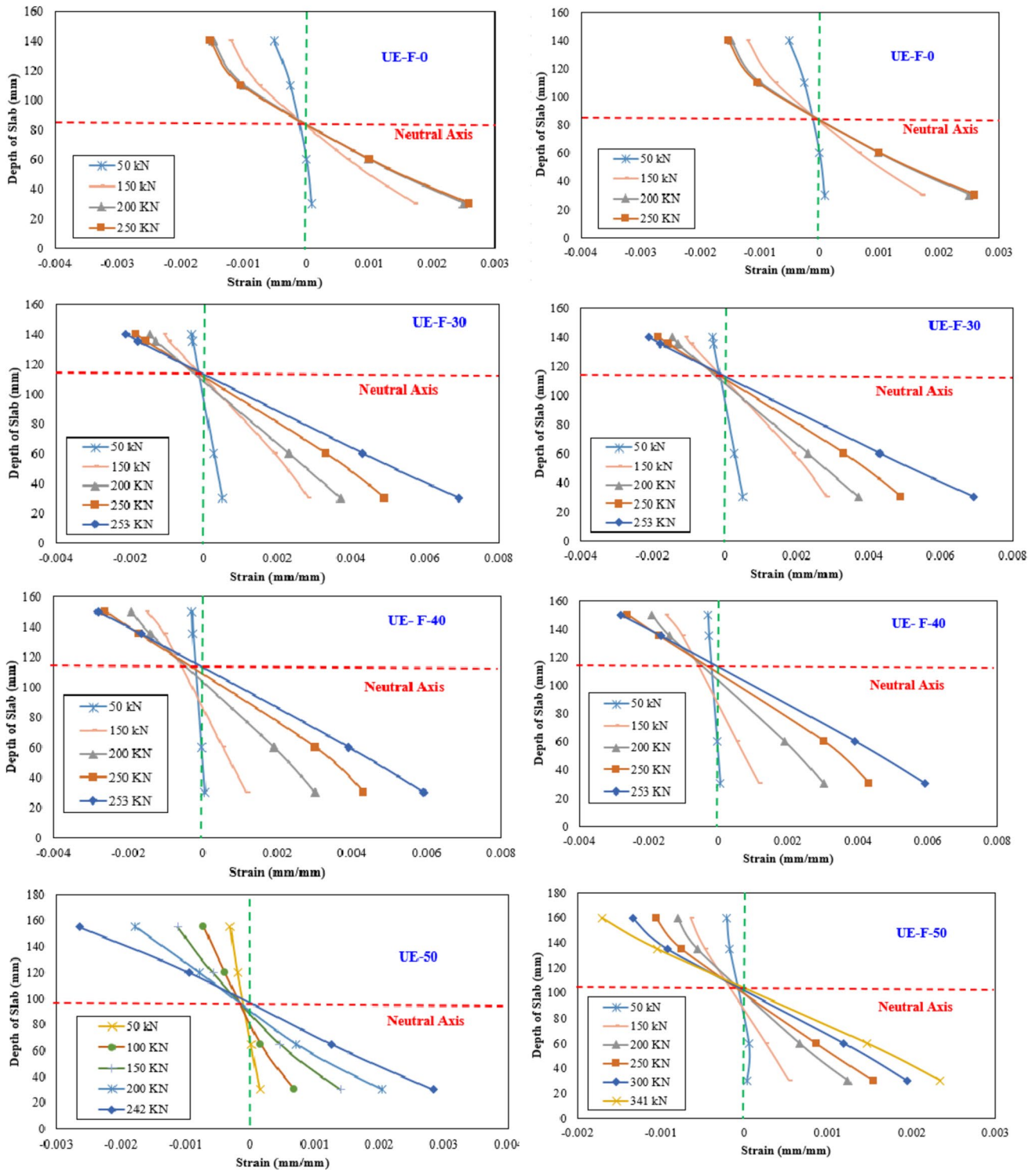
Fig. 14 **a** Strain distribution curves along the depth at mid-span: **a** UE-0; **b** UE-30; **c** UE-40; **d** UE-50; **e** UE-F-0; **f** UE-F-30; **g** UE-F-40; and **h** UE-F-50

Conclusions

This study has investigated a new method for retrofitting RC slabs, involving the use of UHPC in the compression zone alone and the combination of UHPC in the compression zone with FRP in the tension zone (composite UHPC-RC slabs-FRP). The investigation utilized a four-point bending

test. Here are some of the significant findings from this research:

(1) The rebars demonstrated high effectiveness in maintaining the bond between UHPC and NC, with no occurrences of slip at the interface for all tested slabs.

(2) The incorporation of UHPC in the compression zone of the RC slabs markedly enhanced their capacity, concurrently delaying the initiation of cracks up to the top of the slabs.

(3) In the UE series, the failure modes and crack patterns of the composite UHPC-NC were influenced by the presence of UHPC in the compression zone. It is observed that as the thickness of the UHPC layer increased, the modes of failure shifted from brittle shear failure to ductile flexural failure. A significant improvement in ultimate load, up to 64%, was recorded with a 50-mm UHPC layer.

(4) In the UE-F series, all slabs retrofitted with UHPC in the compression zone and FRP in the tension zone failed due to debonding of FRP and shear. The slabs exhibited diagonal and horizontal cracks in the NC followed by debonding of FRP. The results indicate that the UHPC overlay and FRP enhance the ultimate flexural capacity and reduce the ultimate deflection of the retrofitted slabs. The ultimate flexural capacities of the UE-F series were approximately 10.35%–40.08% higher than those of the UE series, respectively. Particularly, the maximum deflection at ultimate flexure of UE-F series is 1.9–2.3 times lowered compared to that of the UE series.

(5) In the UE series, the ductility indexes of the retrofitted slabs increased approximately 2 times with the presence of the UHPC overlay in the compression zone compared to the control slab. However, the presence of FRP in the tension zone in the UE-F series had no influence on the ductility index. When the height of the UHPC layer varies.

(6) The findings of this research are highly promising and demonstrate the potential of utilizing UHPC, as well as combining UHPC with FRP, as an excellent rehabilitation and retrofitting material for structural applications.

For future work, it is essential to investigate the influence of the CFRP layer's thickness and explore methods to prevent debonding of the FRP sheet at the anchorage zone. Additionally, studying the impact of fatigue loading on the behavior of composite UHPC-RC slabs-FRP is crucial and requires both experimental testing and modeling. Conducting experiments on the behavior of composite UHPC-RC slabs with various materials, including steel plate, TRC, and others, also holds promise for future research.

Declarations

Conflict of interest No potential conflict of interest was reported by the authors.

Ethical approval This article's authors did not conduct research involving human subjects or animals.

Informed consent All the authors are aware of this paper.

References

1. Hoang VH, Nguyen QT, Tran AT, Tran TCH, Do TA (2022) Mechanical behavior of the asphalt wearing surface on an orthotropic steel bridge deck under cyclic loading. Case Stud Constr Mater 16:e00836. https://doi.org/10.1016/j.cscm.2021.e00836

2. Yang IH, Joh C, Kim B-S (2010) Structural behavior of ultra high performance concrete beams subjected to bending. Eng Struct 32:3478–3487. https://doi.org/10.1016/j.engstruct.2010.07.017

3. Ho VH, Nguyen NL, Ngo VM (2023) Theoretical calculation of bending capacity of a steel beam–ultra high performance concrete slab composite girder. Transp Commun Sci J. https://doi.org/10.47869/tcsj.74.4.9

4. Abdellatief M, Al-Tam SM, Elemam WE, Alanazi H, Elgendy GM, Tahwia AM (2023) Development of ultra-high-performance concrete with low environmental impact integrated with metakaolin and industrial wastes. Case Stud Constr Mater 18:e01724. https://doi.org/10.1016/j.cscm.2022.e01724

5. Abdellatief M, Elrahman MA, Elgendy G, Bassioni G, Tahwia AM (2023) Response surface methodology-based modelling and optimization of sustainable UHPC containing ultrafine fly ash and metakaolin. Constr Build Mater 388:131696. https://doi.org/10.1016/j.conbuildmat.2023.131696

6. Abdellatief M, Elrahman MA, Abadel AA, Wasim M, Tahwia A (2023) Ultra-high performance concrete versus ultra-high performance geopolymer concrete: mechanical performance, microstructure, and ecological assessment. J Build Eng 79:107835. https://doi.org/10.1016/j.jobe.2023.107835

7. Nguyen MCT, Tran CTN, Nguyen HC, Le DD, Nguyen XH (2024) Experimental investigation on shear behaviours of textile reinforced concrete beams. Eur J Environ Civil Eng. https://doi.org/10.1080/19648189.2023.2214810

8. Hamoda AA, Eltaly BA, Sera RE, Liang QQ (2023) Behavior of reinforced concrete stair slabs strengthened with steel plates and near surface mounted steel bars. Eng Struct 292:116514. https://doi.org/10.1016/j.engstruct.2023.116514

9. Askar MK, Hassan AF, Al-Kamaki YSS (2022) Flexural and shear strengthening of reinforced concrete beams using FRP composites: a state of the art. Case Stud Constr Mater 17:e01189. https://doi.org/10.1016/j.cscm.2022.e01189

10. Graybeal B (2006) Material property characterization of ultra-high performance concrete, FHWA-HRT-06-103, 1-176.

11. El-Helou RG, Haber ZB, Benjamin AG (2022) Mechanical behavior and design properties of ultra-high- performance concrete (open source). ACI Mater J. https://doi.org/10.14359/51734194

12. Brühwiler E (2020) UHPFRC technology to enhance the performance of existing concrete bridges. Struct Infrastruct Eng 16:94–105. https://doi.org/10.1080/15732479.2019.1605395

13. El-Mandouh MA, Elsamak G, RagehHamoda BOA, Abdelazeem F (2023) Experimental and numerical investigation of one-way reinforced concrete slabs using various strengthening systems. Case Stud Constr Mater 18:e01691. https://doi.org/10.1016/j.cscm.2022.e01691

14. Mirdan D, Saleh AR (2022) Flexural performance of reinforced concrete (RC) beam strengthened by UHPC layer. Case Stud Constr Mater 17:e01655. https://doi.org/10.1016/j.cscm.2022.e01655

15. Qasim M, Lee CK, Zhang YX (2023) Flexural strengthening of reinforced concrete beams using hybrid fibre reinforced engineered cementitious composite. Eng Struct 284:115992. https://doi.org/10.1016/j.engstruct.2023.115992

16. Turker K, Torun IB (2020) Flexural performance of highly reinforced composite beams with ultra-high performance fiber reinforced concrete layer. Eng Struct 219:110722. https://doi.org/10.1016/j.engstruct.2020.110722

17. Noshiravani T and Brühwiler E (2013) Experimental investigation on reinforced ultra-high-performance fiber-reinforced concrete composite beams subjected to combined bending and shear, ACI Struct J, 110.

18. Yin H, Teo W, Shirai K (2017) Experimental investigation on the behaviour of reinforced concrete slabs strengthened with ultra-high performance concrete. Constr Build Mater 155:463–474. https://doi.org/10.1016/j.conbuildmat.2017.08.077

19. Al-Osta MA, Isa MN, Baluch MH, Rahman MK (2017) Flexural behavior of reinforced concrete beams strengthened with ultra-high performance fiber reinforced concrete. Constr Build Mater 134:279–296. https://doi.org/10.1016/j.conbuildmat.2016.12.094

20. Abbas EMA, Ge Y, Zhang Z, Chen Y, Ashour A, Ge W, Sun C (2022) Flexural behavior of UHPC beam reinforced with steel-FRP composite bars. Case Stud Constr Mater 16:e01110. https://doi.org/10.1016/j.cscm.2022.e01110

21. Huang Y, Lee M-G, Kan Y-C, Wang W-C, Wang Y-C, Pan W-B (2022) Reinforced concrete beams retrofitted with UHPC or CFRP. Case Stud Constr Mater 17:e01507. https://doi.org/10.1016/j.cscm.2022.e01507

22. Kadhim MMA, Jawdhari A, Nadir W, Cunningham LS (2022) Behaviour of RC beams strengthened in flexure with hybrid CFRP-reinforced UHPC overlays. Eng Struct 262:114356. https://doi.org/10.1016/j.engstruct.2022.114356

23. Abdallah M, Al Mahmoud F, Khalil N, Khelil A (2023) Effect of the strengthening patterns on the flexural performance of RC continuous beams using FRP reinforcements. Eng Struct 280:115657. https://doi.org/10.1016/j.engstruct.2023.115657

24. Liu L, Wan S (2022) Flexural bearing capacity of reinforced concrete beams reinforced with carbon fiber reinforced plastics strips and ultra-high performance concrete layers. Int J Build Pathol Adapt Ahead-Print. https://doi.org/10.1108/IJBPA-04-2022-0056

25. Hoang VH (2023) Experimental study on flexual behavior of reinforced concrete slab strengthened ultra-high-performance concrete. Transp Commun Sci J 74:1100–1109. https://doi.org/10.47869/tcsj.74.9.7

26. De Larrard F, Sedran T (2002) Mixture-proportioning of high-performance concrete. Cem Concr Res 32:1699–1704. https://doi.org/10.1016/S0008-8846(02)00861-X

27. Hoang VH (2011) Interaction fluide-structure: comportement tribologique des matériaux minéraux à base cimentaire à l'état frais, Thesis (PhD) in INSA Rennes, France.

28. Mélinge Y, Hoang VH, Rangeard D, Perrot A, Lanos C (2013) Study of tribological behaviour of fresh mortar against a rigid plane wall. Eur J Environ Civil Eng 17:419–429. https://doi.org/10.1080/19648189.2013.786242

29. Hoang VH, Do TA, Tran AT, Lanos C, Mélinge Y (2023) Effect of electro-osmosis on lubrication of fresh cement paste-based material in contact with a metal wall. Korea-Aust Rheol J 35:157–168. https://doi.org/10.1007/s13367-023-00063-0

30. Yu R, Spiesz P, Brouwers HJH (2014) Mix design and properties assessment of ultra-high performance fibre reinforced concrete (UHPFRC). Cem Concr Res 56:29–39. https://doi.org/10.1016/j.cemconres.2013.11.002

31. Arora A, Aguayo M, Hansen H, Castro C, Federspiel E, Mobasher B, Neithalath N (2018) Microstructural packing- and rheology-based binder selection and characterization for ultra-high performance concrete (UHPC). Cem Concr Res 103:179–190. https://doi.org/10.1016/j.cemconres.2017.10.013

32. Hoang VH (2023) Experimental and numerical study on tensile behavior of ultra-high-performance concrete. Transp Commun Sci J 74(6):709–717. https://doi.org/10.47869/tcsj.74.6.2

33. ASTM-D3039 (2014) Standard test method for tensile properties of polymer matrix composite materials.

34. ASTM-D790–17 (2017) Standard test methods for flexural properties of unreinforced and reinforced plastics and electrical insulating materials.

35. D6272–17e1 A (2020) Standard test method for flexural properties of unreinforced and reinforced plastics and electrical insulating materials by four-point bending.

36. Park R (1989) Evaluation of ductility of structures and structural assemblages from laboratory testing. Bull N Z Soc Earthq Eng 22:155–166. https://doi.org/10.5459/bnzsee.22.3.155-166